ARTICLE

State to State Photodissociation Dynamics of Vibrationally Excited D_2O in B Band†

Shan-yu Han[a], Lin-sen Zhou[a], Dai-qian Xie[a,b]*

a. Institute of Theoretical and Computational Chemistry, Key Laboratory of Mesoscopic Chemistry, School of Chemistry and Chemical Engineering, Nanjing University, Nanjing 210093, China
b. Synergetic Innovation Center of Quantum Information and Quantum Physics, University of Science and Technology of China, Hefei 230026, China

(Dated: Received on June 29, 2015; Accepted on July 25, 2015)

The state-to-state photodissociassion dynamics for the B band of D_2O have been explored from quantum dynamical calculations including the electronic $\tilde{X}$ and $\tilde{B}$ states. The calculations were carried out using a Chebyshev real wave packet method. The calculated absorption spectra, product state distributions, and branching ratios from different initial vibrational states show different dynamic features, due to the different shapes of the vibrational wavefunctions. The initial bending mode (0,1,0) generates two lobes with a shallow minimum on the absorption spectrum and a slight inverted vibrational population of $OD(\tilde{X})$ product at high total energies. The rotational state distributions of $OD(\tilde{X}, v{=}0)$ product are highly inverted and depend weakly on the initial state and total energy. On the other hand, the ro-vibrational distributions of $OD(\tilde{A})$ product strongly oscillate with the total energy, which are dominated by the long-living resonances and depend sensitively on the potential surfaces. The antisymmetric stretching mode (0,0,1) has large $OD(\tilde{A})/OD(\tilde{X})$ branching ratios at high total energies, which indicates that the B band dissociation proceeds mainly via the adiabatic pathway in some cases.

Key words: Photodissociation, D_2O, Vibrationally excited state, Conical intersection, Quantum dynamics

I. INTRODUCTION

The photodissociation dynamics of the water molecule is an important topic in atmospheric and interstellar chemistry [1−3]. The water molecule absorbs a photon in the vacuum ultraviolet region starting by the $\tilde{A}^1B_1 \leftarrow \tilde{X}^1A_1$ transition with a broad continuum around 150−200 nm, which is a fast process and leads to a H atom and an $OH(\tilde{X}^2\Pi)$ radical with a little internal excitation due to the pure repulsive nature of the corresponding potential energy surface (PES). The A band is an excellent example of direct photodissociation and is well understood [4]. The $\tilde{B}^1A_1 \leftarrow \tilde{X}^1A_1$ transition near 130 nm is much more complex, because it involves all three lowest electronic states that are non-adiabatically coupled. In addition to the adiabatical pathway leading to $OH(\tilde{A}^2\Sigma^+)$+H asymptote, there exit two non-adiabatic pathways toward $OH(\tilde{X}^2\Pi)$+H fragments, via the Renner-Teller (RT) coupling between $\tilde{B}$ and $\tilde{A}$ states and two competitive conical intersections (CIs) between $\tilde{B}$ and $\tilde{X}$ states at the linear HOH and HHO geometries causing an interesting quantum interference [5−8]. As a result, the B band can serve as a prototype for understanding nonadiabatic dynamics in polyatomic systems, which has been extensively studied experimentally and theoretically, revealing rich and interesting dynamics [9].

A "holy grail" of photodissocation is laser control of the outcome of a nonadiabatic reaction [10]. Using vibrational pumping the molecule before photoexcitation, different portions of the excited-state PES can be explored, which may be an effective way to control the fragmentation dynamics toward a specific target. For example, strong mode specificity and bond selectivity have been reported in the vibrational mediated photodissociation (VMP) of ammonia via the A band [11−21], which has two product channels $H+NH_2(\tilde{A}^2A_1)$ and $H+NH_2(\tilde{X}^2B_1)$ accessibly via adiabatic and a seams of CIs between $\tilde{X}^1A'$ and $\tilde{A}^1A'$ pathways, respectively. The three-dimensional quantum mechanical studies of VMP of H_2O in the B band have been reported by our group [22]. Our theoretical results demonstrated that the photo-excitation of bending and stretching modes could significantly influence the dissociation dynamics, which yield different

†Dedicated to Professor Qing-shi Zhu on the occasion of his 70th birthday.
*Author to whom correspondence should be addressed. E-mail: dqxie@nju.edu.cn

absorption spectra and branching ratios.

The substitution of hydrogen by deuterium little changes the electronic character of the water molecule, but can significantly influence the photodissociation dynamics, in particular where the nonadiabatic couplings are involved [23−27]. Recently, we have used the two-state coupling model including $\tilde{X}$ and $\tilde{B}$ states to study the D_2O photodissociation in the B band [28], since the RT non-adiabatic coupling has been demonstrated to play a relatively minor role in the dissociation and can be partly compensated by the CI channel [29]. Our results are in excellent agreement with the lastest experimental results, indicating that our new set of diabatic PESs as well as the dynamical calculations are highly reliable. One more interesting aspect is that the related results of D_2O show some quantitative variations from those of H_2O [7, 28, 30].

In order to get a whole picture of D_2O photodissociation in the B band, we employed the two-state coupling model to further investigate the state-to-state photodissociation dynamics of D_2O at its three fundamental vibrational states in this work. The calculated absorption spectra, product state distributions, and branching ratios are compared with the previous results of the ground vibrational state [28].

II. CALCULATION DETAILS

The photodissociation of D_2O in the B band can be described as follows:

$$\mathrm{D_2O}\left(\tilde{X},(v_1,v_2,v_3),J_{K_aK_c}\right)\xrightarrow{h\nu}\mathrm{D_2O}(\tilde{B})\xrightarrow{\text{adiabatic}}\mathrm{D{+}OD}\left(\tilde{A}^2\Sigma^+,v,j\right) \quad (1)$$

$$\xrightarrow{\text{CI}}\mathrm{D_2O}(\tilde{X})\rightarrow\mathrm{D{+}OD}\left(\tilde{X}^2\Pi,v,j\right) \quad (2)$$

where (v_1,v_2,v_3) and $J_{K_aK_c}$ designate a ro-vibrational state of $D_2O(\tilde{X})$. v_1, v_2, and v_3 denote quantum numbers of the symmetric stretching, bending, and antisymmetric stretching modes, respectively. The $OD(\tilde{X}/\tilde{A})$ fragments are labeled by the vibrational (v) and rotational (j) quantum numbers. In this work, the electronic and spin momenta of the parent molecule and fragments were ignored.

Due to the breakdown of the Born-Oppenheimer approximation, it is more convenient in dynamical calculations to use a quasi-diabatic representation for minimizing the derivative coupling [10]. The nuclear Hamiltonian defined in the diabatic representation is given in the matrix form as:

$$\hat{H}=\hat{T}_N\begin{bmatrix}1&0\\0&1\end{bmatrix}+\begin{bmatrix}V_\Sigma&V_{\Sigma\Pi}\\V_{\Sigma\Pi}&V_\Pi\end{bmatrix} \quad (3)$$

where V_Σ, V_Π, and $V_{\Sigma\Pi}$ are the three diabatic PESs and have been developed in our previous work [31]. $\hat{T}_N$ is the nuclear kinetic energy operator and specified in the product H-OH Jacobi coordinates (R, r, γ) as,

$$\hat{T}_N=-\frac{1}{2\mu_R}\frac{\partial^2}{\partial R^2}-\frac{1}{2\mu_r}\frac{\partial^2}{\partial r^2}+\frac{\hat{j}^2}{2\mu_r r^2}+\frac{(\hat{J}-\hat{j})^2}{2\mu_R R^2} \quad (4)$$

where r and R denote the O−D and D−OD distances respectively with μ_r and μ_R as the corresponding reduced masses. $\hat{j}$ is the diatomic rotational angular momentum operator in the Jacobi angle (γ) between vectors $\mathbf{R}$ and $\mathbf{r}$, and $\hat{J}$ is the total angular momentum operator. In our model, the z-axis of the body-fixed (BF) frame was defined along $\mathbf{R}$.

Following our previous work, the photodissociation dynamics of D_2O was investigated using a Chebyshev real wavepacket propagation [32], which is similar to the real method of Gray and Balint-Kurti [33]. The propagation of the diabatic wavepacket was performed in the Chebyshev order (ξ) domain via the three-term recursion relation [34, 35],

$$\Psi_{\xi+1}=D\left(2\hat{H}_{\text{norm}}\Psi_\xi-D\Psi_{\xi-1}\right),\qquad \xi>1 \quad (5)$$

with $\Psi_1{=}D\hat{H}_{\text{norm}}\Psi_0$. The initial wavepacket was set exclusively on the excited diabatic state given by the initial ro-vibrational wavefunction of D_2O multiplied by the $\tilde{B}{\leftarrow}\tilde{X}$ transition dipole moment function $\hat{\mu}$ as $|\Psi_0\rangle=(\hat{e}\times\hat{\mu})\,|\Phi_i\,(r,R,\gamma,E_i)\rangle$, with $\hat{e}$ as the direction of the electronic field of the photon. The Hamiltonian in Eq.(3) was normalized to [−1,1] via $\hat{H}_{\text{norm}}{=}\left(\hat{H}-\bar{H}\right)\Big/\Delta H$. The spectral half-width and mean $\bar{H}{=}(H_{\max}+H_{\min})/2$, $\Delta H{=}(H_{\max}-H_{\min})/2$ of the Hamiltonian were obtained from the spectral extrema, $H_{\max}$ and $H_{\min}$, which can be readily estimated. The damping factor D applied at the grid edges was defined as:

$$D(x)=1,\qquad x<x_d,\ (x=r,R) \quad (6)$$

$$D(x)=\mathrm{e}^{-\alpha(x-x_d)^2},\ x\geq x_d\ (x=r,R) \quad (7)$$

In the asymptotic region, the diabatic state $|\Sigma\rangle$ dissociates to the product $OD(\tilde{A}^2\Sigma^+)$, whereas the diabatic states $|\Pi\rangle$ correlates to the product $OD(\tilde{X}^2\Pi)$. The wavepacket was analyzed at each propagation step and the T matrix elements can be calculated using the relations as follows [36, 37]:

$$C_{vj}^{JKp}(\xi)=\left\langle P_j^K(\gamma)\,\chi_{vj}(r)\right|\Psi_\xi\rangle \quad (8)$$

$$A_{vj}^{JKp}(E)=\frac{1}{2\pi\Delta H\sqrt{1-E_{\text{norm}}^2}}\sum_{\xi=0}^{\infty}(2-\delta_{n0})\cdot\mathrm{e}^{-i\xi\,\arccos E_{\text{norm}}}C_{vj}^{JKp}(\xi) \quad (9)$$

$$T_{vj}^{JKp}(E)=i(-1)^{K-j}\sqrt{1+\delta_{0K}}\left(\frac{\pi k_{vj}}{\mu_R}\right)^{1/2}\cdot\mathrm{e}^{-ik_{vj}R_\infty}A_{vj}^{JKp}(E) \quad (10)$$

DOI:10.1063/1674-0068/28/cjcp1506138

where k_{vj} is the corresponding wave vector and R_∞ is the point where the final state projection is performed. $P_j^K(\gamma)\,\chi_{vj}(r)$ is a product ro-vibrational wavefunction. K is the z component of J in the BF frame and p is the rotational parity. The T matrix elements contain all the information about the photodissociation dynamics. The integral cross section (ICS) can be evaluated as [37, 38],

$$\sigma_{vj}(E) = \frac{4\pi^2\omega}{c}\frac{1}{2J_i+1}\sum_{J=J_i-1}^{J_i+1}\sum_{K}^{J}\frac{\delta(JJ_i1)}{3}T_{vj}^{JKp^*}T_{vj}^{JKp} \tag{11}$$

where ω is the frequency of excitation photon and c is the speed of light. $\delta(JJ_i1)$ was defined in Ref.[38]. The total cross section (absorption spectrum) can be simply obtained using a cosine Fourier transform of the Chebyshev autocorrelation function [32]:

$$\sigma_{\rm tot}(E) = \sum_{v,j}\sigma_{vj}(E) \tag{12}$$

$$= \frac{\pi\omega}{c\varepsilon_0}\frac{1}{\Delta H\pi\sqrt{1-E_{\rm nrom}^2}}\sum_{\xi=0}^{\infty}(2-\delta_{\xi0})\cdot\cos(\xi\arccos E_{\rm norm})\langle\Psi_0|\Psi_\xi\rangle \tag{13}$$

Similar to our previous work, the Hamiltonian including all the Coriolis coupling and wavepacket were represented with a mixed discrete variable representation (DVR) and finite basis representation (FBR). The r and R coordinates were represented by 95 sine-DVR points in [1.2, 6.0]a_0 and 255 sine-DVR points in [1.2, 20.0]a_0, respectively. 100 Legendre functions were used for the angular degree of freedom. We only considered the VMP from the three fundamental vibrational states of $D_2O(\tilde{X}, (v_1, v_2, v_3), 0_{00})$, and the corresponding wavefunctions were calculated by diagonalizing the ground state Hamiltonian with the Lanczos algorithm. The calculated energies for the (1,0,0), (0,1,0), and (0,0,1) vibrational states were found to be 2665.34, 1178.65, and 2779.63 cm^{-1}, respectively, which are very close to the corresponding experimental values of 2671.65, 1178.38, and 2787.72 cm^{-1} [39, 40]. In keeping with the spectroscopy selection rule, all the initial wave packets on the excited state have a total angular momentum of J=1. The converged photodissociation cross sections were reached by carrying out a total of 25000 Chebyshev propagation steps with the analysis line placed at R_∞=11.5a_0.

III. RESULTS AND DISCUSSION

A. Total cross section

In Fig.1, the calculated total absorption cross sections (TCSs) from three fundamental vibrational states of D_2O are compared with our previous theoretical result from the ground vibrational state, which agrees well with the experimental spectrum [28]. The TCSs are plotted as a function of the total energy, defined as $E_{\rm tot}$=$E_{\rm int}((v_1,v_2,v_3),0_{00})$+$h\nu$, where $E_{\rm int}$ is the vibrational energy of the ground state and $h\nu$ is the photon energy. The arrows in Fig.1 show four undulating vibronic peaks of the TCS from the (0,0,0) vibrational state, which were chosen to study the effect of the initial vibrational wave functions on the dissociation dynamics of D_2O via the B band at specific energies.

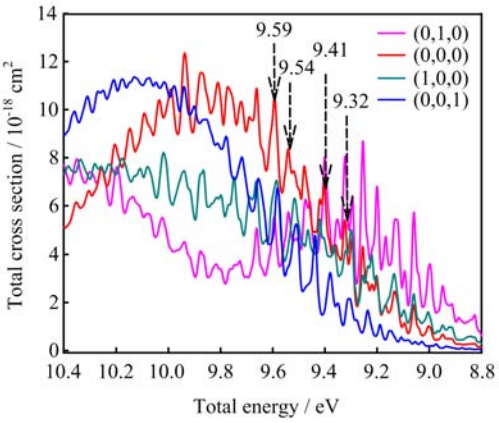

FIG. 1 Calculated total cross sections from three fundamental vibrational states of D_2O as a function of total energy together with the previous result from the ground vibrational state. The arrows indicate the energies at which product state distributions are calculated.

The TCSs in Fig.1 are similar to those of H_2O from the same vibrational state, exhibiting diffuse vibronic structures superimposed on a broad band and most pronounced amplitudes on the low energy tail. The various features of the broad bands in the four TCSs are mainly attributed to the different shapes of the initial vibrational wavefunctions. From the classical reflection principle [41], one can expect that the (0,1,0) TCS shows clearly two lobes with a shallow minimum, since the (0,1,0) wave function has one node along the Jacobi angle (γ) coordinate. On the other hand, compared to the TCSs of H_2O, those of D_2O have smaller widths and less pronounced amplitudes of the undulating structures, and the spacing between the resonances is smaller and the overlapping is stronger for D_2O [42, 43]. These resonances are supported by the potential well formed by the CI around the linear DOD region and are grouped in clusters with a complicated bending-stretching couplings, thus making the exact mechanism of the resonance structures unclear [31, 42, 44, 45].

B. Product state distribution of OD($\tilde{X}$)

Figure 2 shows the calculated vibrational state distributions of OD($\tilde{X}$) from the four vibrational states

DOI:10.1063/1674-0068/28/cjcp1506138

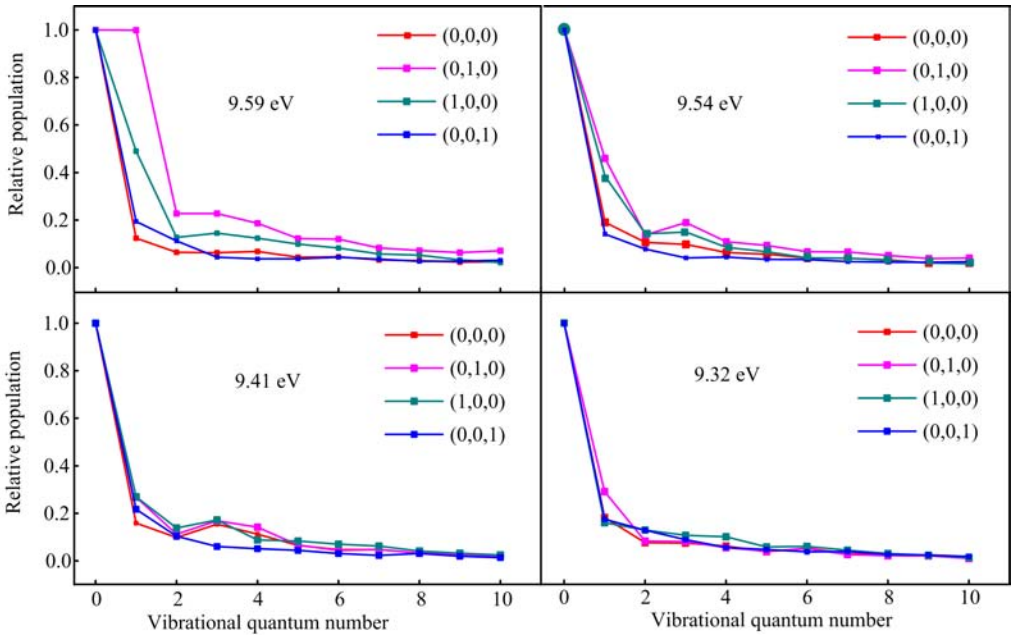

FIG. 2 Calculated relative vibrational state distributions of the OD($\tilde{X}$) product from four vibrational states of D_2O at four total energies. The populations of v=0 have been normalized.

of D_2O at four total energies. Similar to the VMP of H_2O [22], the vibrational state distributions from (0,0,0), (1,0,0), and (0,0,1) states depend weakly on the total energy and are dominant by OD($\tilde{X}$, v=0), although many vibrationally excited states are also populated. It is now well understood that the v=0 fragment is largely produced by the fast and direct trajectories passing through DOD CI located at (R_{OD_1}, R_{OD_2}, $\angle$DOD)=(1.853a_0, 3.056a_0, 180°) with the nonreactive OD bond length still maintaining its initial lengths, whereas the minor vibrational excited states are presumably formed by the indirect trajectories passing through DDO CI at (R_{OD_1}, R_{OD_2}, $\angle$DOD)=(1.986a_0, 3.681a_0, 0°) where the OD bond is significantly elongated from its equilibrium geometry [31]. The dominance of OD($\tilde{X}$, v=0) also appears in the vibrational state distribution from the (0,1,0) state at three lower total energies, but the populations of v=0 and v=1 are almost equal at a higher energy of 9.59 eV, since the (0,1,0) wave packet covers a large angular regions of the $\tilde{B}$ state potential, a part of which can easily pass through DDO CI channel at higher total energy above the barrier between the two CIs [22].

The calculated rotational state distributions for the OD($\tilde{X}$, v=0) products from the four vibrational states at four total energies are displayed in Fig.3. The distributions are highly inverted with a maximum peak around j=55, close to the highest allowed rotational state. Due to the reduced mass difference between D and H atoms, the maximum rotational quantum numbers of OD($\tilde{X}$, v=0) are larger than those of OH($\tilde{X}$, v=0) from the dissociation of H_2O in the B band. The extremely high rotational excitation is induced by the strong angular force at $\tilde{B}$←$\tilde{X}$ CIs along the nonadiabatic dissociation pathway. As shown in Fig.3, the rotational state distributions of OD($\tilde{X}$, v=0) mainly depend on the large torque along the nonadiabatic channels and are weakly affected by the initial vibrational states and total energy. Thus the rotational state distributions from the four vibrational states have similar dynamical behavior. It is also interesting to note that the distributions show clear intensity oscillations around j=45, similar to those observed at 121.6 nm, which can be attributed to a quantum interference of the outgoing wavepackets from the $\tilde{B}$ to $\tilde{X}$ surfaces via the two linear DOD and DDO CIs [7].

C. Product state distribution of OD($\tilde{A}$)

The calculated vibrational state distributions of OD($\tilde{A}$) as a function of the total energy above the OD($\tilde{A}$, v=0) threshold are given in Fig.4. Since the OD($\tilde{A}$) fragments are generated via the adiabatic pathway and have a high energy threshold, only a few low-lying vibrational states are populated over the whole energy range of the B band. The calculated threshold energies for v=1 and v=2 fragments are 9.47 and 9.73 eV, respectively. The distributions from the four initial vibrational states for each vibrational state of OD($\tilde{A}$) show similar trends. The vibrational excited state populations (v>1) have a sharp rise just above the energy threshold, since more energy is available for these adiabatic products at high total energies. All the

DOI:10.1063/1674-0068/28/cjcp1506138

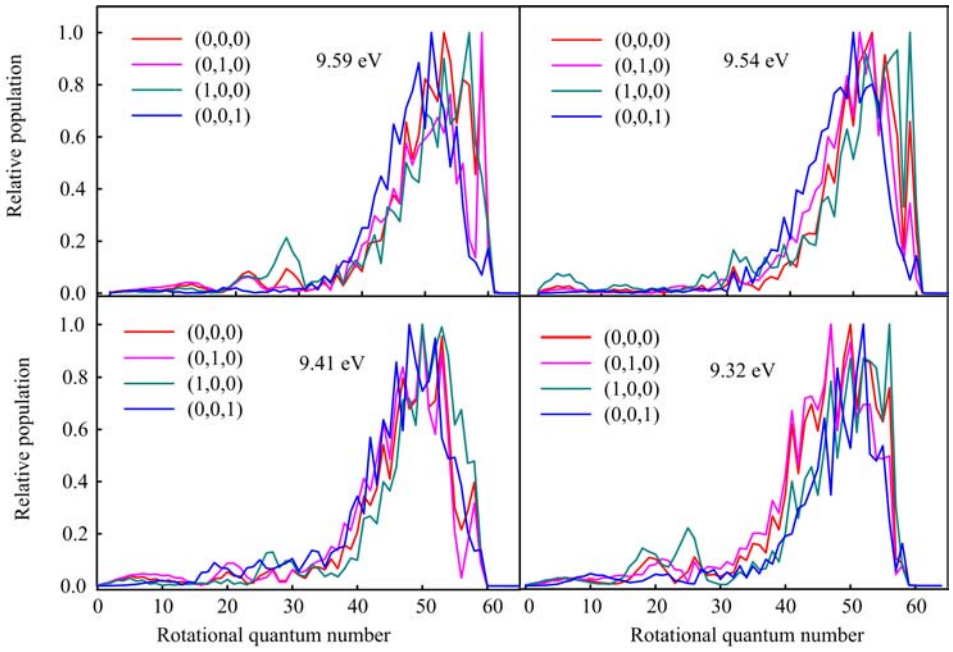

FIG. 3 Calculated rotational state distributions for OD($\tilde{X}$, v=0) fragments from four vibrational states of D_2O at four total energies. The maximum value of the population is set to 1.

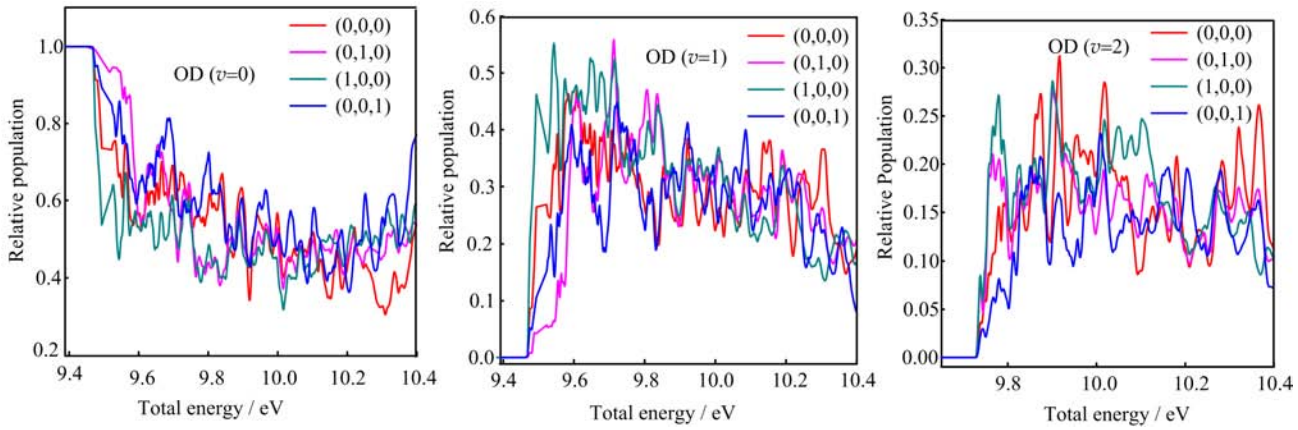

FIG. 4 Calculated vibrational state distributions for OD($\tilde{A}$) fragments from four vibrational states of D_2O as a function of total energy.

distributions show strong oscillations, indicating the existence of many long-living resonances.

Figure 5 presents the calculated rotational state distributions of OD($\tilde{A}$, v=0) from the four vibrational states at four total energies. Because of the smaller angular anisotropy of the $\tilde{B}$ state surface along the adiabatic pathway, the OD($\tilde{A}$, v=0) products are less rotationally excited than its ground state counterparts in Fig.3. The rotational populations show a rather random distribution with various oscillations, which are very sensitive to the energy and initial vibrational state. As discussed previously [28, 29, 31, 45, 46], this behavior stems from the metastable resonances, which depend sensitively on the PES and can not be accurately characterized up to now.

D. Branching ratio

The branching ratio between the $\tilde{A}$ and $\tilde{X}$ states of the products plays an important role in the B band photodissociation and can serve as an effective probe of the $\tilde{B}$ state PES in the Franck-Condon region. In our previous work [28, 29, 31], the calculated branching ratios for H_2O and D_2O from the ground vibrational state were in good agreement with the available experiments values, which confirms the accuracy of our diabatic PESs in the Franck-Condon region. Figure 6 shows the cal-

DOI:10.1063/1674-0068/28/cjcp1506138

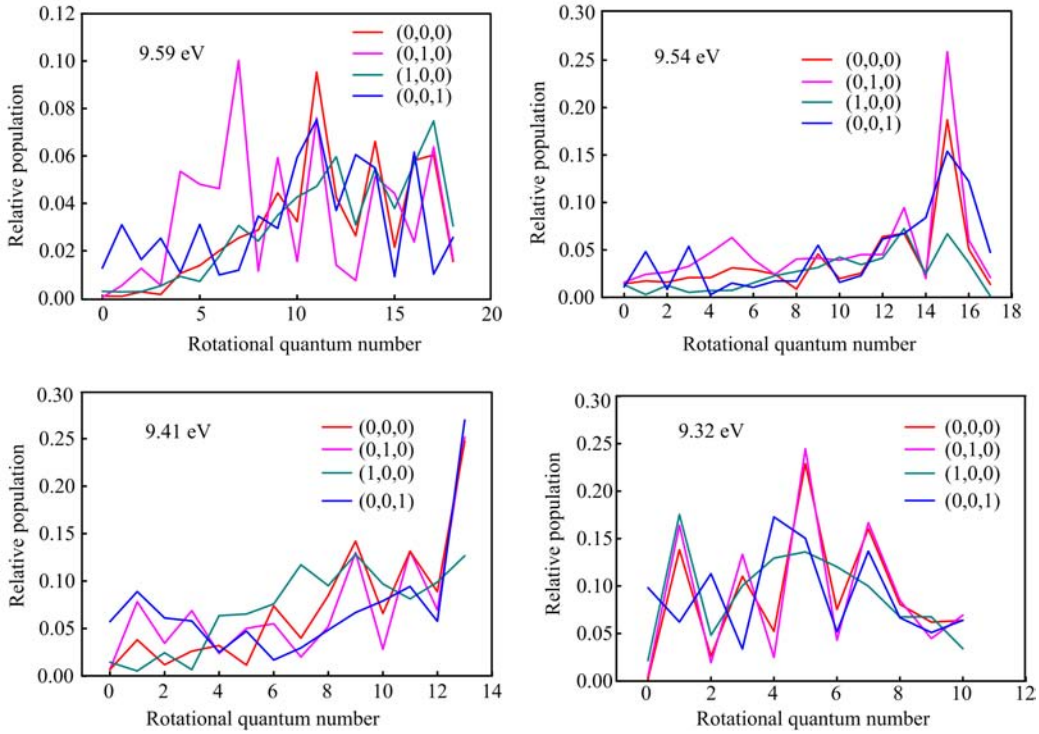

FIG. 5 Calculated rotational state distributions for OD($\tilde{A}$, v=0) fragments from four vibrational states of D_2O at four total energies. The total populations are normalized.

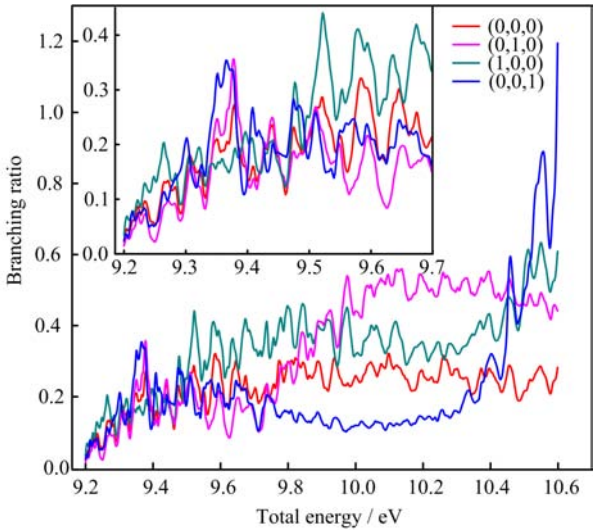

FIG. 6 Calculated OD($\tilde{A}$)/OD($\tilde{X}$) branching ratios from four vibrational states of D_2O as a function of total energy.

culated branching ratios of OD($\tilde{A}$)/OD($\tilde{X}$) from four vibrational states as a function of the total energy. Similar to the vibrational state distributions of OD($\tilde{A}$) discussed above, the calculated branching ratios oscillate with the total energy, due to the resonances. The four branching ratios are a quick rising function of the energy at the beginning above the OD($\tilde{A}$) dissociation threshold. For (0,0,0), (1,0,0), and (0,0,1) states, the branching ratios change slowly at high energies. But for the (0,1,0) state, the branching ratio starts to rise again at 9.7 eV and is then steady at about 0.45−0.5 after 10.0 eV, which becomes significantly larger than those of the other states at the energy range between 10.0 and 10.14 eV. All the branching ratios show that the OD($\tilde{X}$) channel is dominant over the OD($\tilde{A}$) channel, due to the strong CI nonadiabatic coupling. However, the branching ratio of (0,0,1) state increases almost linearly and exceeds the ratio of 1.0 at higher total energy tail, which means that the adiabatic channel becomes important in some cases.

IV. CONCLUSION

Vibrationally mediated photodissociation of D_2O in the B band allows the exploration of the excited state PES in regions that are not accessible from the ground vibrational state. In this work, we report the state-to-state photodissociation dynamics of D_2O at its three fundamental vibrational states, based on an accurate quantum mechanical model including CI nonadiabatic coupling and our recently developed coupled *ab initio* PESs.

The calculated absorption spectra from different vibrational states differ from each other, due apparently to the different shapes of the initial vibrational wave-

DOI:10.1063/1674-0068/28/cjcp1506138

functions. The vibrational distributions of OD($\tilde{X}$) from (0,0,0), (1,0,0), and (0,0,1) states are dominant by the v=0 state, whereas the (0,1,0) vibrational distributions are slight inverted at higher total energy range. The rotational distributions of OD($\tilde{X}$, v=0) are highly inverted and depend weakly on the energy and initial vibrational states, because of the same mechanism dominated by the conical intersections. The ro-vibrational distributions of OD($\tilde{A}$) from different vibrational states present strong oscillations, indicating the existence of many long-living resonances. The calculated branching ratios OD($\tilde{A}$)/OD($\tilde{X}$) show that the nonadiabatic pathway dominates for the (0,0,0), (1,0,0) and (0,0,1) states throughout the whole energy range. This trend also exists for the (0,1,0) state at low energy range, but the adiabatic pathway becomes dominant at some higher energies. We wish our study could stimulate further theoretical and experimental investigations on this important system.

V. ACKNOWLEDGMENTS

This work supported by the National Natural Science Foundation of China (No.21133006, No.21273104, and No.91221301) and the Ministry of Science and Technology (No.2013CB834601).

[1] R. P. Wayne, *Chemistry of Atmospheres*, Oxford: Oxford University Press, (1991).
[2] P. Andresen, Astron. Astrophys. **154**, 42 (1986).
[3] B. P. Bonev and M. J. Mumma, Astrophys. J. **653**,788 (2006).
[4] V. Engel, V. Staemmler, R. L. Vander Wal, F. F. Crim, R. J. Sension, B. Hudson, P. Andresen, S. Hennig, K. Weide, and R. Schinke, J. Chem. Phys. **96**, 3201 (1992).
[5] R. N. Dixon, D. W. Hwang, X. F. Yang, S. Harich, J. J. Lin, and X. Yang, Science **285**, 1249 (1999).
[6] S. A. Harich, D.W. Hwang, X. Yang, J. J. Lin, X. Yang, and R. N. Dixon, J. Chem. Phys. **113**, 10073 (2000).
[7] S. A. Harich, X. Yang, D. W. Hwang, J. J. Lin, X. Yang, and R. N. Dixon, J. Chem. Phys. **114**, 7830 (2001).
[8] L. Zhou, D. Xie, and H. Guo, J. Chem. Phys. **142**, 124317 (2015).
[9] K. Yuan, R. N. Dixon, and X. Yang, Acc. Chem. Res. **44**, 369 (2011).
[10] D. R. Yarkony, Chem. Rev. **112**, 481 (2012).
[11] J. P. Reid, R. A. Loomis, and S. R. Leone, J. Chem. Phys. **112**, 3181 (2000).
[12] J. P. Reid, R. A. Loomis, and S. R. Leone, J. Phys. Chem. A **104**, 10139 (2000).
[13] A. Bach, J. M. Hutchison, R. J. Holiday, and F. F. Crim, J. Chem. Phys. **116**, 9315 (2002).
[14] A. Bach, J. M. Hutchison, R. J. Holiday, and F. F. Crim, J. Chem. Phys. **116**, 4955 (2002).
[15] A. Bach, J. M. Hutchison, R. J. Holiday, and F. F. Crim, J. Chem. Phys. **118**, 7144 (2003).
[16] A. Bach, J. M. Hutchison, R. J. Holiday, and F. F. Crim, J. Phys. Chem. A **107**, 10490 (2003).
[17] H. Akagi, K. Yokoyama, and A. Yokoyama, J. Chem. Phys. **118**, 3600 (2003).
[18] H. Akagi, K. Yokoyama, and A. Yokoyama, J. Chem. Phys. **120**, 4696 (2004).
[19] M. L. Hause, Y. H. Yoon, and F. F. Crim, J. Chem. Phys. **125**, 174309 (2006).
[20] C. Xie, X. Zhu, J. Ma, D. R. Yarkony, D. Xie, and H. Guo, J. Chem. Phys. **142**, 091101 (2015).
[21] J. Ma, C. Xie, X. Zhu, D. R. Yarkony, D. Xie, and H. Guo, J. Phys. Chem. A **118**, 11926 (2014).
[22] G. S. M. Lin, L. Zhou, and D. Xie, J. Phys. Chem. A **118**, 9220 (2014).
[23] S. A. Harich, X. Yang, X. Yang, and R. N. Dixon, Phys. Rev. Lett. **87**, 253201 (2001).
[24] R. N. Dixon, T. A. A. Oliver, L. Cheng, Y. Cheng, K. Yuan, and X. Yang, J. Chem. Phys. **138**, 104306 (2013).
[25] S. A. Harich, X. F. Yang, X. Yang, R. van Harrevelt, and M. C. van Hemert, Phys. Rev. Lett. **87**, 263001 (2001).
[26] L. Cheng, K. Yuan, Y. Cheng, Q. Guo, X. Yang, and R. N. Dixon, Mol. Phys. **108**, 905 (2010).
[27] L. Cheng, K. Yuan, Y. Cheng, Q. Guo, T. Wang, D. Dai, X. Yang, and R. N. Dixon, J. Phys. Chem. A **115**, 1500 (2011).
[28] L. Zhou, G. S. M. Lin, and D. Xie, J. Chem. Phys. **139**, 114303 (2013).
[29] L. Zhou, B. Jiang, D. Xie, and H. Guo, J. Phys. Chem. A **117**, 6940 (2013).
[30] Y. Cheng, L. Cheng, Q. Guo, K. Yuan, D. Dai, and X. Yang, J. Chem. Phys. **134**, 104305 (2011).
[31] B. Jiang, D. Xie, and H. Guo, J. Chem. Phys. **136**, 034302 (2012).
[32] H. Guo, J. Chem. Phys. **108**, 2466 (1998).
[33] S. K. Gray and G. G. Balint-Kurti, J. Chem. Phys. **108**, 950 (1998).
[34] V. A. Mandelshtam and H. S. Taylor, J. Chem. Phys. **103**, 2903 (1995).
[35] R. Chen and H. Guo, J. Chem. Phys. **105**, 3569 (1996).
[36] R. Chen and H. Guo, Comput. Phys. Commun. **119**, 19 (1999).
[37] G. G. Balint-Kurti, Adv. Chem. Phys. **128**, 249 (2004).
[38] G. G. Balint-Kurti and M. Shapiro, Chem. Phys. **61**, 137 (1981).
[39] C. L. Lin and J. H. Shaw, J. Mol. Spectrosc. **66**, 441 (1977).
[40] N. Papineau, J. M. Flaud, C. Camy-Peyret, and G. Guelachvili, J. Mol. Spectrosc. **87**, 219 (1981).
[41] R. Schinke, *Photodissociation Dynamics*, Cambridge: Cambridge University Press, (1993).
[42] R. van Harrevelt and M. C. van Hemert, J. Chem. Phys. **112**, 5787 (2000).
[43] B. M. Cheng, C. Y. Chung, M. Bahou, Y. P. Lee, L. C. Lee, R. van Harrevelt, and M. C. van Hemert, J. Chem. Phys. **120**, 224 (2004).
[44] K. Weide and R. Schinke, J. Chem. Phys. **90**, 7150 (1989).
[45] M. von Dirke, B. Heumann, K. Kühl, T. Schröder, and R. Schinke, J. Chem. Phys. **101**, 2051 (1994).
[46] B. Jiang, D. Xie, and H. Guo, J. Chem. Phys. **134**, 231103 (2011).

DOI:10.1063/1674-0068/28/cjcp1506138